The ATPase cycle of human muscle myosin II isoforms: Adaptation of a single mechanochemical cycle for different physiological roles

Received for publication, June 17, 2019, and in revised form, July 28, 2019 Published, Papers in Press, August 6, 2019, DOI 10.1074/jbc.RA119.009825

Chloe A. Johnson[‡], Jonathan Walklate[‡], Marina Svicevic[§], Srboljub M. Mijailovich[¶], Carlos Vera[‖], Anastasia Karabina[‖], Leslie A. Leinwand[‖1], and Michael A. Geeves[‡2]

From the [‡]School of Biosciences, University of Kent, Canterbury CT2 7NJ, United Kingdom, the [§]Faculty of Science, University of Kragujevac, Kragujevac 34000, Serbia, the [¶]Department of Biology, Illinois Institute of Technology, Chicago, Illinois 60616, and the [‖]BioFrontiers Institute and Department of Molecular, Cellular, and Developmental Biology, University of Colorado, Boulder, Colorado 80309

Edited by Enrique M. De La Cruz

Striated muscle myosins are encoded by a large gene family in all mammals, including humans. These isoforms define several of the key characteristics of the different striated muscle fiber types, including maximum shortening velocity. We have previously used recombinant isoforms of the motor domains of seven different human myosin isoforms to define the actin·myosin cross-bridge cycle in solution. Here, we present data on an eighth isoform, the perinatal, which has not previously been characterized. The perinatal is distinct from the embryonic isoform, appearing to have features in common with the adult fast-muscle isoforms, including weak affinity of ADP for actin·myosin and fast ADP release. We go on to use a recently developed modeling approach, MUSICO, to explore how well the experimentally defined cross-bridge cycles for each isoform in solution can predict the characteristics of muscle fiber contraction, including duty ratio, shortening velocity, ATP economy, and load dependence of these parameters. The work shows that the parameters of the cross-bridge cycle predict many of the major characteristics of each muscle fiber type and raises the question of what sequence changes are responsible for these characteristics.

Muscle myosin in all mammals consists of a variety of isoforms, each expressed from its own gene (see Table 1 and references therein). There are 10 such genes in the human genome and one pseudogene. All of the striated muscle myosin sequences are very highly conserved, but each has functional differences, and these differences are required for normal muscle function because myosin isoform-specific null mice can have profound phenotypes (1). Further, disease-causing mutations in six of the 10 genes have been reported (2, 3). The expression of these genes is regulated temporally and spatially and can be affected by physical activity, animal species, and hormonal status. Each myosin isoform confers distinct contractile characteristics to each muscle fiber type (4, 5). These characteristics include maximum shortening velocity, rate of ATP usage, economy of ATP usage, and velocity at which power output is maximal. Other parameters, such as maximal force per cross-bridge or step size, are much less variable (4, 5). How each myosin is tuned for its specific function is not well-understood. Also poorly understood is how changes in the amino acid sequence of each myosin bring about the functional changes. As a first step to understand how striated muscle myosin has evolved to have distinct physiological roles, we first needed to understand how the ATP driven cross-bridge cycle varies between the isoforms. Toward that end, we recently published a complete characterization of the kinetics of the ATPase cycle for the motor domains of six adult human muscle myosin isoforms and the embryonic isoform (6–8) (see Table 1). Here, we extend this data set to include the first study of the human perinatal myosin isoform. We show here that the perinatal isoform is quite distinct from the embryonic form and has more in common with adult fast-muscle isoforms.

With this large set of isoform data, it is possible to examine the extent to which differences in the ATPase cycle for each isoform can predict the differences in mechanochemical properties of muscle fibers expressing them. Here, we use the recently developed MUSICO modeling approach (9, 10) to predict the contraction characteristics of each muscle fiber type and compare the predictions with published data for single muscle fibers expressing single myosin isoforms.

Using MUSICO, we recently reexamined the actin myosin-S1 ATPase cycle of fast rabbit muscle using both fast kinetic methods and steady-state ATPase assays to establish the primary parameters of an eight-step actin·myosin cross-bridge cycle (Fig. 1) (9). These parameters were then used with the addition of the overall ATPase parameters for the cycle, the k_{cat} (or V_{max}), and K_{app} (concentration of actin needed for half-

This work was supported by National Institutes of Health Grants GM29090 (to L. A. L.) and HL117138 (to L. A. L.) and European Union Horizon 2020 Research and Innovation Programme under Grant agreement No. 777204, SILICOFCM (to M. A. G., J. W., and S. M. M.). This article reflects only the author's view. The European Commission is not responsible for any use that may be made of the information it contains. L. A. L. owns stock in MyoKardia, Inc and has received research funding from the company. The authors declare that they have no conflicts of interest with the contents of this article.

This article contains Tables S1–S5 and Figs. S1–S5.

[1] To whom correspondence may be addressed: BioFrontiers Institute and Dept. of Molecular, Cellular, and Developmental Biology, University of Colorado, Boulder, CO 80309. E-mail: leslie.leinwand@colorado.edu.

[2] To whom correspondence may be addressed: School of Biosciences, University of Kent, Canterbury CT2 7NJ, United Kingdom. Tel.: 44-1227827597; E-mail: m.a.geeves@kent.ac.uk.

Table 1
Summary of isoforms

Isoform	Human gene	Human tissue expression[a]	Maximum shortening velocity in muscle fiber[b]	Light chains[c]	Expression tags on heavy chain
α-Cardiac (α)	*MYH6*	Atrial myocardium		Endogenous mouse	His_6
β-Cardiac/slow muscle I (β)	*MYH7*	Ventricular myocardium/slow skeletal	0.330 ± 0.022	Human MYL3	His_6 on MYL3
Embryonic (Emb)	*MYH3*	Fetal skeletal and regenerating muscles		Endogenous mouse	His_6
Perinatal (Peri)	*MYH8*	Fetal skeletal and regenerating muscles		Endogenous mouse	His_6
Extraocular (Exoc)	*MYH13*	Extraocular and laryngeal muscles		None	e-GFP, His_6
IIa	*MYH2*	Fast skeletal	1.401 ± 0.101	Endogenous mouse	e-GFP, His_6
IIb	*MYH4*	Not expressed		Endogenous mouse	e-GFP, His_6
IId	*MYH1*	Fast skeletal	3.022 ± 0.935	Endogenous mouse	e-GFP, His_6

[a] Ref. 39.
[b] Ref. 14.
[c] Endogenous mouse light chains are a combination of MLC1A, MLC3F, MLC1F, and MLC2F.

maximum ATPase rates) to model the complete cycle in solution. This allowed the occupancy of each state of the cycle to be predicted as a function of actin concentration. The occupancies calculated were then used to predict the duty ratio (DR;[3] the proportion of the cycle myosin bound to actin), the expected maximal velocity of contraction (V_0, in a motility assay or muscle sarcomere shortening) as a function of actin concentration, and the effect of a 5-pN load on state occupancies for a single motor. To test this approach, we compared the information obtained for rabbit fast-muscle myosin with two human cardiac myosin isoforms (α and β) that we had characterized previously (6). These illustrated how the cycle was altered to define myosins with different velocities and different sensitivities to load. Whereas the duty ratio was largely unchanged among isoforms, the ATPase cycling rates and predicted velocities were altered in line with published experimental data. The effect of load reduced the predicted velocities and ATPase rates but to differing extents. Here, we have added in predictions about the economy of ATP usage during rapid shortening and while holding a 5-pN load.

In the current study, the analysis described above has been extended to four additional adult, fast-skeletal, human isoforms (IIa, IIb, IId, and extraocular (ExOc)) together with two developmental isoforms: embryonic (Emb) and perinatal (Peri) myosins. The analysis reveals that the relative velocities predicted for the isoforms vary widely (9-fold). Duty ratios vary over a narrow 2-fold range, whereas the economy of ATP usage varies 4–5-fold. Experimental data for these values are only available for a limited number of isoforms but, where available, are compatible with our predictions. The extent to which these ATPase cycle studies can predict the properties of contracting muscle for both the well-defined and unstudied isoforms (*e.g.* ExOc and Peri) is discussed.

Results and discussion

We have modeled, using MUSICO, the complete ATPase cycle for all isoforms listed in Table 1. The modeling used the previously published values for the rate and equilibrium constants (Table S1) that have defined the cycle shown in Fig. 1. The best-fit parameters are listed in Table 2. In all cases, the measured constants were defined with a precision of at least ±20%. The limitations of this precision on the modeling will be considered below, but in general, varying any of the parameters by ±20% has a limited effect on the cycle, in most cases altering the occupancy of each state by much less than 20%. One new set of experimental data is presented here, that for the Peri isoform. Data collection was identical to that presented for all other isoforms, with the measured parameters listed in Table S1 and the predicted occupancies in Table S2.

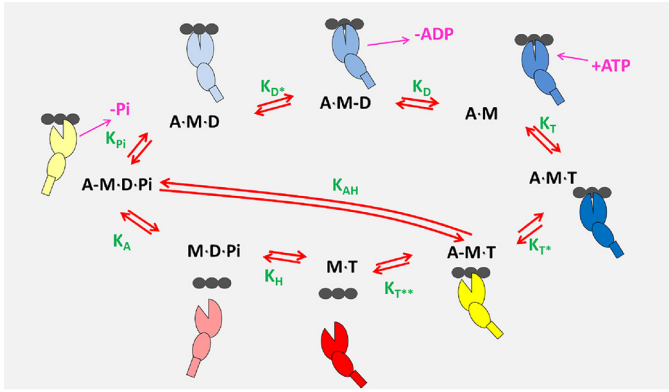

Figure 1. ATP-driven actomyosin cross-bridge cycle. The *black circles* represent an actin filament composed of three actin monomers. Myosin is shown as *two ellipses* and a *rod*; the *larger ellipse* represents the upper and lower 50 k domains, the *smaller ellipse* and *rod* representing the converter domain, lever arm, and light-chain binding region. Myosin in a strongly attached, force-holding state is represented in *blue*, weakly attached in *yellow*, and detached in *red shades*. *Green* characters are the equilibrium constants for each step defined in the direction of ATP hydrolysis (*clockwise*).

Using a combination of best-fit and measured values for the cycle, the occupancy of each state in the cycle was calculated at three different actin concentrations: [actin] = K_{app} (the actin concentration required for 50% of the V_{max} of the ATPase) and [actin] = $3K_{app}$ and $20K_{app}$ (actin concentration required for 75 and 95% of V_{max}, respectively). A range of actin concentrations was chosen because it is not known what the appropriate actin concentration is in muscle fibers. Fig. 2 presents the calculated occupancies for each state in the cycle as *pie charts* for each isoform. The *color scheme* of the *pie charts* matches that of the ATPase cycle states shown in Fig. 1, where *red shades* represent detached states, *yellow shades* represent weakly attached states, and blue shades represent strongly attached states.

α- and β-cardiac isoforms

For β-cardiac myosin, at low actin concentrations ([actin] = K_{app}), the detached state M·D·P_i predominated (*pale red shade*; ~45–50%), with similar amounts of the detached M·T and the

[3] The abbreviations used are: DR, duty ratio; pN, piconewton(s); ExOc, extraocular; Emb, embryonic; Peri, perinatal.

Table 2

Fitted rate and equilibrium constants of the ATPase cycle

Constants are highlighted to show which are fitted (blue), which are measured (red), and which are derived from assumption (black on yellow background) or detailed balance (purple on yellow background). Buffer conditions are as follows: 25 mM KCl, 20 mM MOPS, 5 mM $MgCl_2$, and 1 mM NaN_3. Note that k_D values in red were measured with an ADP displacement with excess ATP assay. For the other isoforms that have a low affinity of ADP for actin·S1, the ADP release rate will be faster than the maximal rate of ATP-induced actin·S1 dissociation and therefore too fast to be measured by ADP displacement.

A. Equilibrium Constants

	Units	*α-S1*	*β-S1*	*Emb*	*Peri*	*ExOc*	*IIa*	*IIb*	*IId*
K_{app}	μM	67.8	39.55	39	20.6	18.6	22.5	7	7.9
k_{cat}	s^{-1}	18	5.94	7	29.9	29.6	26.4	43.1	32.9
K_A	μM^{-1}	0.011	0.0107	0.0164	0.0241	0.035	0.0293	0.0874	0.0913
K_{pi}	mM	100	100	100	100	100	100	100	100
K_{D*}		50	0.167	0.2	50	50	50	50	50
K_D	μM	197	36	71.43	100	100	100	100	100
K_T	μM^{-1}	0.004	0.003	0.0119	0.0068	0.00834	0.0045	0.0042	0.005
K_{T*}		150	154	77.7	85.6	138	135	146	122.8
K_{T**}	μM	1000	1000	1000	1000	1000	1000	1000	1000
K_H		4.1	8.9	6.3	16.6	35.7	23.2	29.2	31.3
K_{AH}		52.76	63.145	43.6	34	55	47.5	30	32.5

B. Forward Rate Constants

	Units	*α-S1*	*β-S1*	*Emb*	*Peri*	*ExOc*	*IIa*	*IIb*	*IId*
k_A	$\mu M^{-1}s^{-1}$	10.68	10.75	16.4	24.1	3.51	2.93	8.47	9.13
k_{Pi}	s^{-1}	32.14	15.95	13.1	69.2	50.1	44.5	86	52.3
k_{D*}	s^{-1}	100	59	22	700	400	400	1000	1000
k_D	s^{-1}	1970	1000	1000	1000	1000	1000	1000	1000
k_T	$\mu M^{-1}s^{-1}$	27.6	10.05	10.13	10.67	10.27	10.37	10.1	10.9
k_{T*}	s^{-1}	1800	1543	777	856	1380	1350	1460	1228
k_{T**}	s^{-1}	1000	1000	1000	1000	1000	1000	1000	1000
k_H	s^{-1}	77.2	12.5	82.4	66.6	107.2	92.8	116.7	125.2
k_{AH}	s^{-1}	79.1	12.6	87.2	68	110	95	120	130

C. Backward Rate Constants

	Units	*α-S1*	*β-S1*	*Emb*	*Peri*	*ExOc*	*IIa*	*IIb*	*IId*
k_{-A}	s^{-1}	1000	1000	1000	1000	1000	1000	1000	1000
k_{-Pi}	$mM^{-1}s^{-1}$	0.321	0.159	0.13	0.692	0.501	0.445	0.86	0.523
k_{-D*}	s^{-1}	2	354	110	14	8	8	20	20
k_{-D}	$\mu M^{-1}s^{-1}$	10	27.8	14	10	10	10	10	10
k_{-T}	s^{-1}	6597	3349	851.5	1569.2	1230.9	2304.4	2396.6	2179.3
k_{-T*}	s^{-1}	12	10	10	10	10	10	10	10
k_{-T**}	$\mu M^{-1}s^{-1}$	1	1	1	1	1	1	1	1
k_{-H}	s^{-1}	19	1.4	13	4	3	4	4	4
k_{-AH}	s^{-1}	1.5	0.2	2	2	2	2	4	4

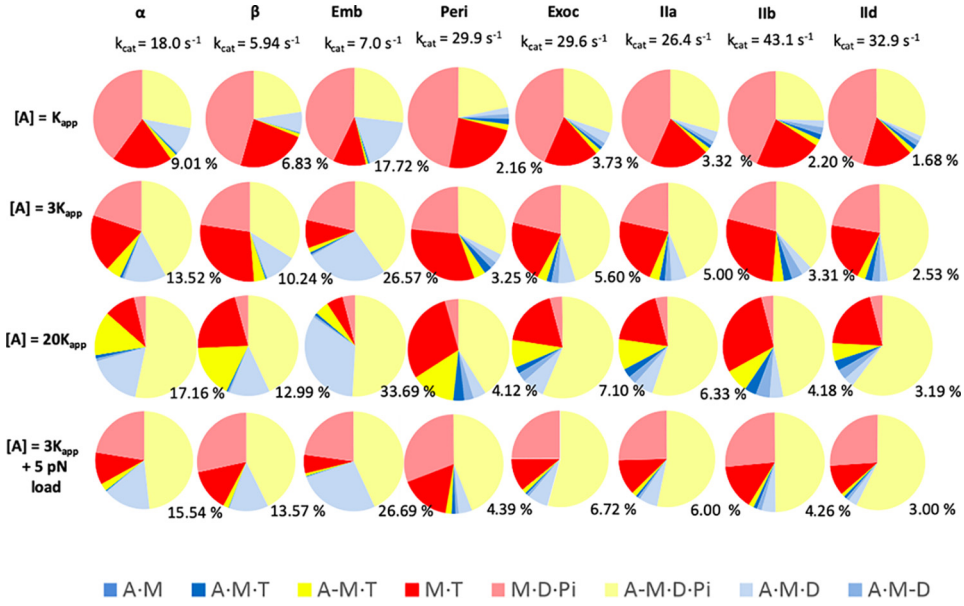

Figure 2. Fractional occupancies of each state in the ATPase at three different actin concentrations, [A] = K_{app}, 3K_{app}, and 20K_{app}, for each isoform and at [A] = 3K_{app} plus 5-pN load. *Colors* of the *pie chart* match those of Fig. 1. The percentage value next to each chart gives the percentage of each cycle spent as the force-holding A·M·D state.

weakly attached A-M·D·P_i state (each ~25%). Only 6.8% of the myosin is strongly attached as A·M·D, the predominant force-holding state. All other species in the cycle have very low occupancy in the steady state. As actin concentration increased (to 3K_{app}/75% V_{max} and 20K_{app}/95% V_{max}), the total occupancy of the detached states fell to ~50% and then 25%, and the weakly attached A-M·ATP and A-M·D·P_i increased from <25 to 35% and then >50% as expected. The strongly attached force-holding states are dominated by the pale blue A·M·D state, which increased from 6.8% at low actin concentrations to 10 and 13.0% as the actin concentration approached saturation. Thus, the DR is dominated by A·M·D and lies between 0.07 and 0.14, depending upon the actin concentration, at the zero load experienced in these solution assays. A similar pattern was observed for the human α-myosin except for a slightly higher level of the A·M·D state, between 9.0 and 17.6%, depending upon the actin concentration and a DR of 0.1 to 0–0.19.

Table 2 and Fig. 2 list the measured k_{cat} values (ATPase cycling rates) for the α- and β-isoforms. Despite quite similar occupancies of the intermediates in the cycle, the cycling rates are very different; α-cardiac turns over ATP almost 3 times faster than β-cardiac. The predicted velocities were 2.25-fold faster for the α- *versus* the β-isoform (Fig. 3 and Table 3), which is similar to measured values (11). This calculation assumes an average 5-nm step for both. This result has implications for the economy of ATP usage, which will be discussed below (see Fig. 5).

Single-molecule laser trap assays have provided estimates of the load dependence of the ADP release rate constant (k_{D^*}) for human β-myosin and indicate that this rate constant slows down by a factor of ~3 for a load of 5 pN (see "Materials and methods" (12, 13)). We argued that a similar load dependence is expected on the force-generating step/P_i release step (k_{Pi} in Fig. 1), and for the values used in the cycle, a 3-fold reduction in k_{Pi} is required to slow the ATPase cycling rate under load, as has been reported for contracting muscle fibers (14, 15). Slowing both rate constants (k_{Pi} and k_{D^*}) down by a factor of 3 allows us to explore how the cycle would change under a 5-pN load, approaching the load that might be expected during isometric contraction of a fiber. The results are illustrated in the *last row* of the *pie charts* in Fig. 2 for an actin concentration of 3K_{app},

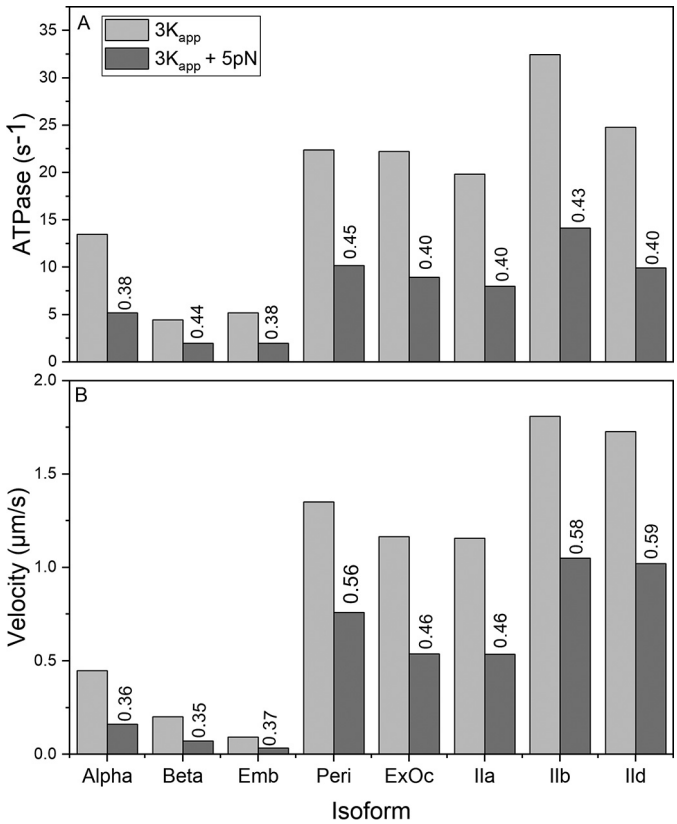

Figure 3. Plots of the estimated ATPase and V_0 values at [actin] = 3K_{app} and the effect of a 5-pN load. The *numbers* give the loaded value as a fraction of the unloaded value.

Table 3
Predicted cross-bridge cycle parameters at three actin concentrations from the modeled ATPase cycle
Buffer conditions were as for Table 2.

Isoform	[Actin]	ATPase	Detached	Weakly attached	Strongly attached	Duty ratio	Velocity
	μM	s^{-1}					$\mu m\ s^{-1}$
α	K_{app} = 67.8	9.00	0.60	0.30	0.10	0.10	0.45
	$3K_{app}$ = 203.4	13.50	0.38	0.47	0.15	0.15	0.45
	$20K_{app}$ = 1356	17.14	0.14	0.67	0.19	0.19	0.45
	$3K_{app}$ + load	5.27	0.33	0.51	0.16	0.16	0.16
β	K_{app} = 39.55	2.97	0.73	0.20	0.073	0.073	0.20
	$3K_{app}$ = 75	4.46	0.57	0.32	0.11	0.11	0.20
	$20K_{app}$ = 500	5.66	0.30	0.56	0.14	0.14	0.20
	$3K_{app}$ + load	1.97	0.47	0.39	0.14	0.14	0.071
Embryonic	K_{app} = 39	3.51	0.54	0.28	0.19	0.19	0.095
	$3K_{app}$ = 117	5.27	0.30	0.42	0.28	0.28	0.095
	$20K_{app}$ = 780	6.68	0.093	0.55	0.35	0.35	0.095
	$3K_{app}$ + load	1.89	0.29	0.44	0.27	0.27	0.035
Perinatal	K_{app} = 20.6	14.92	0.71	0.23	0.055	0.055	1.36
	$3K_{app}$ = 61.8	22.41	0.55	0.36	0.083	0.083	1.35
	$20K_{app}$ = 412	28.44	0.34	0.55	0.11	0.11	1.34
	$3K_{app}$ + load	10.19	0.47	0.46	0.067	0.067	0.76
Extraocular	K_{app} = 18.6	14.82	0.62	0.312	0.064	0.064	1.17
	$3K_{app}$ = 55.8	22.24	0.43	0.47	0.095	0.095	1.17
	$20K_{app}$ = 372	28.16	0.23	0.65	0.12	0.12	1.16
	$3K_{app}$ + load	8.94	0.37	0.55	0.083	0.083	0.54
IIa	K_{app} = 22.5	13.21	0.63	0.31	0.057	0.057	1.16
	$3K_{app}$ = 67.5	19.82	0.44	0.48	0.086	0.086	1.16
	$20K_{app}$ = 450	25.11	0.23	0.66	0.11	0.11	1.15
	$3K_{app}$ + load	7.98	0.37	0.55	0.074	0.074	0.54
IIb	K_{app} = 7	21.59	0.67	0.27	0.060	0.060	1.81
	$3K_{app}$ = 21	32.47	0.5	0.41	0.090	0.090	1.81
	$20K_{app}$ = 140	41.0	0.34	0.55	0.11	0.11	1.80
	$3K_{app}$ + load	14.12	0.42	0.51	0.067	0.067	1.049
IId	K_{app} = 8	16.47	0.62	0.33	0.048	0.048	1.73
	$3K_{app}$ = 24	24.77	0.42	0.50	0.072	0.072	1.73
	$20K_{app}$ = 160	31.27	0.25	0.66	0.091	0.091	1.72
	$3K_{app}$ + load	9.93	0.37	0.58	0.049	0.049	1.02

and the predicted effect on the ATPase rates and velocity of shortening are illustrated in Fig. 3. There is no measurement of the load dependence of ADP release for any isoform other than β-cardiac. For the purposes of illustration throughout, we assume a similar load dependence for all isoforms to understand how a load may influence the cycle differently based on the observed differences in the cycle rate constants. The data for the effect of load on the state occupancy, the ATPase rate, and the velocity are presented in Figs. 2 and 3 and Table 3. For both α and β, the ATPase cycling rates were reduced by approximately a factor of 3, whereas the occupancy of the A·M·D state increased from 10.2 to 13.6% for human β and 13.5 to 15 .5% for α. This implies that for an ensemble of myosins (in a thick filament or sarcomere), the α-myosin would maintain a higher occupancy of the force-holding states. Note, however, for β-myosin, the occupancy of A·M·D increases by one-third under load, whereas for α-myosin, the occupancy increases by only about one-seventh.

Embryonic isoform

The complete experimental data set for the human Emb isoform was published in 2016 (8), and the published data are reproduced in Table S1. The results of the modeling are presented in Figs. 2–4 in the same format as for the α- and β-isoforms for ease of comparison.

What is immediately striking in the Emb data set is that, although the k_{cat} values for the Emb isoform and β-isoform are similar (7.0 and 5.9 s^{-1}, respectively), there are marked differences in the occupancy of the force-holding A·M·D state (*pale blue*; Fig. 1). Whereas the detached M·D·P_i (*pale red*) and A-M·D·P_i (*pale yellow*) appear similar for β and Emb, the detached M·T (*red*) state was much smaller and the A·M·D state (*pale blue*) was much larger for Emb than for β (*e.g.* A·M·D = 26.5% for Emb *versus* 10.24% at [actin] = $3K_{app}$). This difference was less marked when compared with the α-isoform. This large difference in A·M·D occupancy and duty ratio are brought about through differences in the contribution of three steps to the overall cycling speed (k_{cat}): the hydrolysis step k_H, the phosphate release step k_{Pi}, and the ADP release step k_{D^*}. For β-myosin, k_H and k_{Pi} are comparable at 2–3-fold k_{cat}, whereas k_{D^*} is 10-fold larger than k_{cat} (see Table 4). Thus, as seen in Fig. 2 for the β-isoform at high actin concentration ([actin] = $20K_{app}$), the predominant states are the ATP states M·T and A-M·T (together 45%), the weakly bound A-M·D·P_i (35%), and A·M·D (12.9%). In the case of Emb, k_{cat} is similar to that of β, but the balance of the cycle is quite different: k_H is $10k_{cat}$, and k_{Pi} and k_{D^*} are now comparable at 2–3-fold k_{cat}. Thus, the ATP states M·T and A-M·T are much smaller than k_{D^*}, whereas the A-M·D·P_i (51%) and A·M·D (33%) states predominate, and thus a much larger DR is observed for Emb myosin.

The higher occupancy of the force-holding A·M·D state implies that the Emb isoform would be much better at holding loads than either of the two cardiac isoforms discussed so far. Assuming a similar load-holding capacity for each cross-bridge independent of the isoform, then there are almost twice as many cross-bridges present in the steady-state for Emb myosin, which suggests that a fiber expressing Emb myosin would need

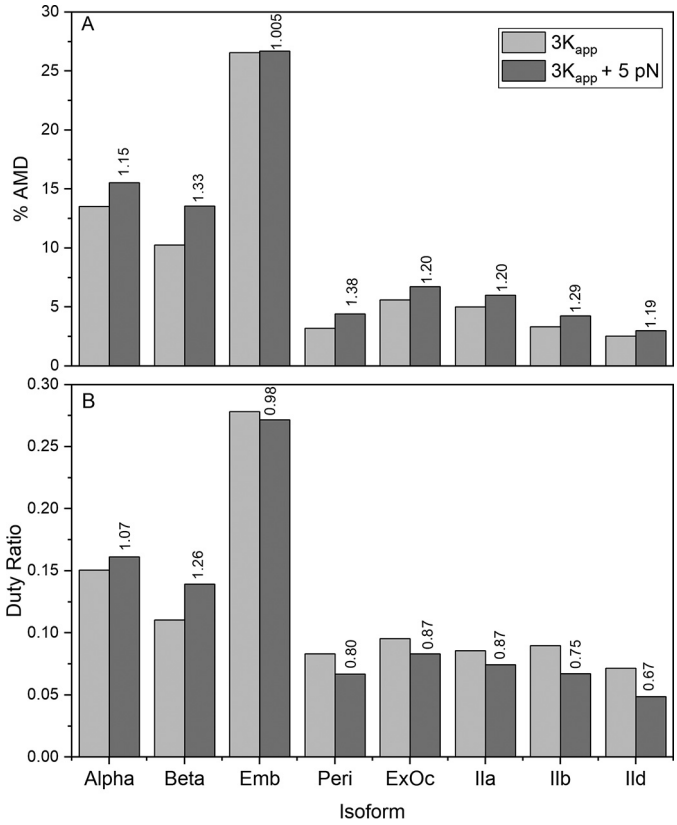

Figure 4. The estimated value of the duty ratio and the occupancy of the main force-holding state A·M·D at [actin] = 3K_{app} and the effect of a 5-pN load. The *numbers* with each isoform give the 5-pN loaded value as a fraction of the unloaded value.

Table 4

Balance of significant rate constants around the ATPase cycle

Note that the slowest step (gray background) is, in each case, ~2 times the k_{cat} value. If this step is largely irreversible (true for k_{Pi}, not always true for k_H), then ~50% of the myosin will occupy the state before this slow step ($k_{cat} = \theta \cdot k$, where θ is the fractional occupancy of that state and k is the rate constant for the breakdown of that state. The second slowest step in all cases (yellow background) is ~3–4 times k_{cat}, and because $\theta = k_{cat}/k$ then θ ~0.25. The third slowest step in each case (blue background) is ~ 10 times k_{cat}, so the occupancy of the relevant state will be approximately 0.1.

Isoform	k_{cat}	k_{Pi}/k_{cat}	k_{D^*}/k_{cat}	k_H/k_{cat}
α	18.00	1.78	5.56	4.28
β	6.00	2.67	9.83	2.07
Emb	7.00	1.87	3.14	11.71
Peri	29.90	2.31	23.4	2.23
Exoc	29.60	1.69	13.51	3.72
IIa	26.40	1.74	15.15	3.60
IIb	43.10	2.09	23.20	2.78
IId	32.40	1.64	30.86	4.01

to activate half the number of cross-bridges (per sarcomere or per thick filament) to hold the same load as a fiber expressing β-myosin. At the whole-fiber or whole-muscle level, the differences in the packing of the filaments would need to be considered.

In contrast to β or α, the presence of a 5-pN load on Emb has almost no effect on the occupancy of the force-holding A·M·D state or the duty ratio. This was unexpected, but a closer examination of the effect of load suggests that because k_{D^*} and k_{Pi} are both similar and dominate the ATPase cycling rate, when both are reduced to a similar extent by load, ATPase cycling is reduced by a factor of 3, but the balance of states around the cycle does not change significantly.

Perinatal isoform

Like Emb, Peri is found in developing and regenerating muscle (2, 16). No biochemical kinetic study of this isoform has been published. Using the C2C12 expression system, we have expressed the motor domain and completed a kinetic analysis as described previously for the other isoforms. Details of the measurements are given in Figs. S1–S4. The measured values for the steps in the ATPase cycle are listed in Table S1. The data do show distinct differences compared with the both the cardiac and Emb isoforms discussed so far.

As the Peri and Emb myosins are both developmental isoforms, a comparison between these is drawn here. A full comparison can be seen in Table S1. In the absence of actin, the Peri S1 had an almost 3-fold slower second-order rate constant of ATP binding to S1 compared with the Emb isoform (4.5 μM^{-1} s^{-1} *versus* 12.5 μM^{-1} s^{-1}). The maximum rate of ATP binding ($k_H + k_{-H}$) is almost 50% slower for the Peri than for the Emb (68.7 s^{-1} *versus* 130 s^{-1}). This is assumed to measure the ATP hydrolysis step. The Peri actin·S1 had a maximum rate of dissociation (k_{+T^*}) of 856 s^{-1} and is similar to the Emb S1 (777 s^{-1}). However, the ATP binding affinity (K_T), and hence the second-order rate constant ($K_T k_{+T^*}$), was almost 2-fold tighter than that of Emb (146.5 μM *versus* 84.3 μM Peri and Emb, respectively). The crucial difference between the two developmental isoforms is the ADP release rate (k_{+D^*}), which is considerably faster (>700 s^{-1}) than the Emb isoform (22 s^{-1}). A slow ADP release rate is indicative of a slow-type isoform, such as β and Emb, whereas the Peri is more like the fast skeletal isoforms (α, IIa, IIb, IId, and ExOc). However, as shown in Fig. S2, the rate constant for ADP release (k_D = 700 s^{-1}) is only marginally slower than the maximum rate of actin dissociation by ATP (k_{T^*} = 856 s^{-1}). We have assigned this to k_{D^*}, but it could equally be assigned to k_D.

The ATPase of the Peri isoform is much faster than Emb, with a k_{cat} of almost 30 s^{-1}, and the rapid release of ADP from A·M·D suggests a fast-type myosin (17). The results of the modeling are shown in Figs. 2–4.

Modeling the cycle shows a similar pattern to the α- and β-myosins but with some key differences. The occupancy of the force-holding, pale blue, A·M·D state (*pale blue*) is much smaller for Peri (~4.1% at [A] = 20K_{app}) compared with α (17%) or β (13%), resulting in a smaller DR (0.11) than for β (0.14). The difference in DR could be considered small, but examination of the *pie charts* in Fig. 2 shows a redistribution among the strongly attached states with the presence of significant amounts of the strongly attached states, A·M-D (~2.8%) and A·M·T (~3.5%) in addition to A·M·D. The presence of other strongly attached states appears to be a feature of the fast-type myosins and will be discussed further when the fast adult myosins are considered.

Similar to the result for the Emb isoform, the change in occupancy observed here for Peri is the result of changes in the balance between k_{Pi}, k_{D^*}, and k_H and their contributions to k_{cat}. Whereas the rate of the hydrolysis step, controlled by k_H, is much faster for Peri at 68.7 s^{-1} than for β (13.9 s^{-1}), it is only

twice the value of k_{cat}. This means that the M·T and A-M·T states dominate at all actin concentrations considered, even more than is the case for β-myosin.

The estimate of velocity for this isoform is 1.35 $\mu m \cdot s^{-1}$, much faster than for α (0.45 $\mu m \cdot s^{-1}$) or β (0.2 $\mu m \cdot s^{-1}$). But this depends upon the assignment of k_{D^*} to 700 s^{-1}. If instead this is k_D, then there would be a missing value of k_{D^*} which could be much lower than 700 s^{-1} and result in a much lower velocity.

Fast skeletal isoforms

The adult fast skeletal isoforms, IIa, IIb, and IId, form a closely related group of myosins, and in humans they have ~92% sequence identity in the motor domain (18). The ExOc is also believed to be a fast-muscle isoform based on contractile velocity of extraocular and pharyngeal muscles (19, 20). However, because it is only found in specialized muscle fibers expressing multiple isoforms, little is known about its biochemical and mechanical properties. It is ~85% identical to the adult fast isoforms. The experimental data for these four isoforms were published in two papers. Resnicow *et al.* (21) published the first ever data on a set of recombinant human isoforms, and Bloemink *et al.* (7) followed this with a more detailed biochemical kinetic study of the same isoforms. The data in Table S1 are a summary of these studies.

Notably, like many larger mammals, humans have not been found to express any IIb protein, although the gene is intact and theoretically capable of expressing protein. The IIb we characterized is thus the only human IIb to have been studied. The fact that its properties appear similar to IIa and IId suggests that the gene has not degenerated significantly, despite not being expressed.

The k_{cat} values for the four isoforms (26 – 43 s^{-1}) are similar to that of Peri (29.9 s^{-1}) and much faster than those for the cardiac and Emb isoforms. As might have been expected, these four fast isoforms show a very similar pattern of occupancy of the states in the cycle (Fig. 2 and Fig. S2), with IIb being slightly different from the other three isoforms. The IIb isoform has a higher occupancy of the MT state and correspondingly lower A-M·D·P_i weakly attached state at high actin concentrations. All four have low occupancy of the A·M·D state (<10% in each case) but with significant variation among the four, varying from 2.5 to 5.6% at [actin] = $3K_{app}$. As seen for the Peri isoform, the DR is not dominated by the A·M·D state; the other strongly attached states (A·M-D, A·M-T) contribute equally to the DR. We set the fast isomerization steps controlling ADP release and actin dissociation arbitrarily as a fast event at 1000 s^{-1}. It is possible that, for these very fast myosins, this value of 1000 s^{-1} is too slow and should be considerably faster. We increased these values to 2000 or 3000 s^{-1} individually or as a group and repeated the modeling. This made little difference to the overall balance of the cycle (see Table S5 for the data set for myosin IId and IIb), with only those intermediates closely associated with the modified rate constant changed, if at all. For all other intermediates, the change was very small and always <10% of the initial value. The strongly attached states remained significantly occupied. The presence of these additional strongly attached states has implications for the DR and how sensitive the cycle is to load. This will be considered further below.

Before considering the implications of the modeling for understanding the different mechanochemical cycles and the role for which each isoforms has been optimized, we should first consider the limitations of the data sets used. There are limited amounts of the protein available for the assays used to define the ATPase cycle, and for good experimental reasons, all data sets were not collected under identical conditions. The early experiments (all fast isoforms) were done at 20 °C and 0.1 M KCl to make a better comparison with physiological conditions. Later, the conditions were changed to 25 mM KCl, as this lower salt concentration was required to generate more reliable actin-activated ATPase data. The data presented for β-myosin were collected at 20 °C at both 100 and 25 mM KCl (6, 22) and allowed us to make corrections between salt conditions for each measured parameter. Similar studies have been published for the rabbit IIa isoform at both salt concentrations, and the corrections required were similar (6, 9). Similarly, there is an extensive collection of temperature dependence data on the β-isoform, from different sources, and for rabbit fast-muscle myosin (23–27). The observation that the corrections are similar for both the fast IIa and the β-cardiac isoforms supports our assumption that the corrections will be similar for each of the closely related isoforms used here; however, this remains an assumption. The measured values are all listed in Table S1, and the corrected values are used in Table 2.

We state under "Materials and methods" that we tested the robustness of our fitting by varying key fitted parameters by ±20%, and these have been published for the cardiac isoforms (9). The supporting information (Table S4) shows representative data for the Emb isoform where one of K_D^*, k_{D^*}, K_{T^*}, k_{T^*}, k_{-D}, or k_H was varied and all others were refitted. Most parameters are changed by very little; those that change by >10% are highlighted in Table S4 and are only those values directly linked to the altered parameter.

Having defined the ATPase and cross-bridge cycle for each of the eight isoforms, we will now consider the implications of the different cycles for the contraction of muscle fibers containing each of these isoforms. Specifically, we will explore the maximum shortening velocity, the load dependence of the cycle, and the economy of ATP utilization.

Maximum velocity of shortening, load dependence, and economy of ATP usage

The V_{max} of shortening (V_0; zero load) of a muscle fiber expressing a single isoform can be estimated from the lifetime (τ) of the strongly attached force-holding state (predominantly AMD) and the individual step size of the working stroke,

$$V_0 = d/\tau \quad \text{(Eq. 1)}$$

From our modeling, τ can be calculated from the equation, τ = DR/ATPase rate, at any actin concentration. Because DR and ATPase rates have very similar dependence on actin concentrations (both proportional to the fractional saturation of myosin with actin), τ and hence V_0 are independent of actin concentration in this model. This means that the ATPase rate and velocity are not directly related except at saturating actin concentrations. The calculation of the V_0 is identical for a con-

tracting muscle fiber and velocity of actin movement in a motility assay, often measured in the absence of load. The model is therefore consistent with the observation that V_0 is independent of the degree of activation of a muscle and only a very small number of myosin cross-bridges are required to achieve V_0. For the purposes of the arguments set out below, we have assumed the working stroke, *d*, to be 5 nm for each isoform.

The equation above assumes that the velocity is limited by the lifetime of the strongly attached states, which, in the model used here, is controlled by the rate of cross-bridge detachment after completing the working stroke. This has been demonstrated to be true for the relatively slow β-type myosin, where the ADP release rate constant (k_{D^*}) is easily measured. The same is true for the slow Emb isoform. For all other isoforms, the ADP release rate constant has not been measured because either the rate constant is too fast for current methods or the relevant A·M·D complex cannot be easily formed by simply mixing ADP with A·M. The equilibrium K_{D^*} in Fig. 1 lies too far toward the A·M-D complex, and little (<5%) A·M·D is formed. For fast rabbit muscle myosin, the value of K_{D^*} was estimated as ~50 (28). Thus, we have good estimates of ADP release from β-cardiac and Emb myosin. For α, Peri, and all fast-muscle isoforms, we have to estimate the ADP release based upon reasoned argument. If ADP release is too fast, then the lifetime and steady-state occupancy of the force-holding state becomes too small, and a muscle would be unable to hold much force. For example, a 1% occupancy of the force-holding state would mean only three force-holding cross-bridges for a fully activated 300-myosin thick filament. If the rate constant is too slow, the velocity becomes smaller than that observed experimentally. Here, we have set that value for these fast fibers at the minimal possible, compatible with the expected velocities.

As noted above, fast-muscle myosins have a higher predicted occupancy of other strongly attached states (*dark blue*), not just the A·M·D state. When k_D was doubled, it had little effect on the occupancy of states in the cycle or the overall ATPase rates, but velocity was increased by 15–20%, and there was a 10% decline in the DR because of a ~10% fall in the A·M-D state. The system does remain, however, a detachment-limited model.

Fig. 3*B* plots the predicted V_0 values for each isoform and indicates there is an ~20-fold range of velocities from Emb (0.09 μm·s^{-1}) to IId (1.66 μm·s^{-1}). The order of predicted velocities and their values relative to Emb velocity are as follows: Emb, 1; β, 2; α, 4; Peri, 8; IIa and ExOc, 12; IId and IIb, 20. Thus, our analysis of the cross-bridge cycle predicts Emb to be both the slowest of the isoforms and the one most capable of holding large steady-state loads (*i.e.* longest lifetime of the A·M·D state and the highest occupancy of A·M·D in the steady state). In contrast, IId was the fastest isoform and has the lowest DR and, hence, lowest force-holding capacity.

The assumption of a 3-fold reduction in the rate constants for P_i and ADP release (k_{Pi} and k_{D^*}) induced by a 5-pN load predicts that for each isoform, the different cycle characteristics result in different sensitivities of velocity to load. This effect of the cycle characteristics would remain true even if the measured load sensitivity varied for each isoform. The slower isoforms α, β, and Emb have the highest sensitivity, with V_0 being reduced by 2.7–2.8-fold. The velocity of ExOc, IIa, and Peri are reduced 2.1-fold, whereas the fastest isoforms IId and IIb show only a 1.6–1.7-fold reduction. This reflects the relative importance of the A·M-D and A·M-T strongly attached states. In the current model, we have assumed that the fast events (rapid ADP release (K_D), ATP binding (K_T), and the ATP-induced dissociation of actin (K_{T^*} and $K_{T^{**}}$) are not directly affected by load.

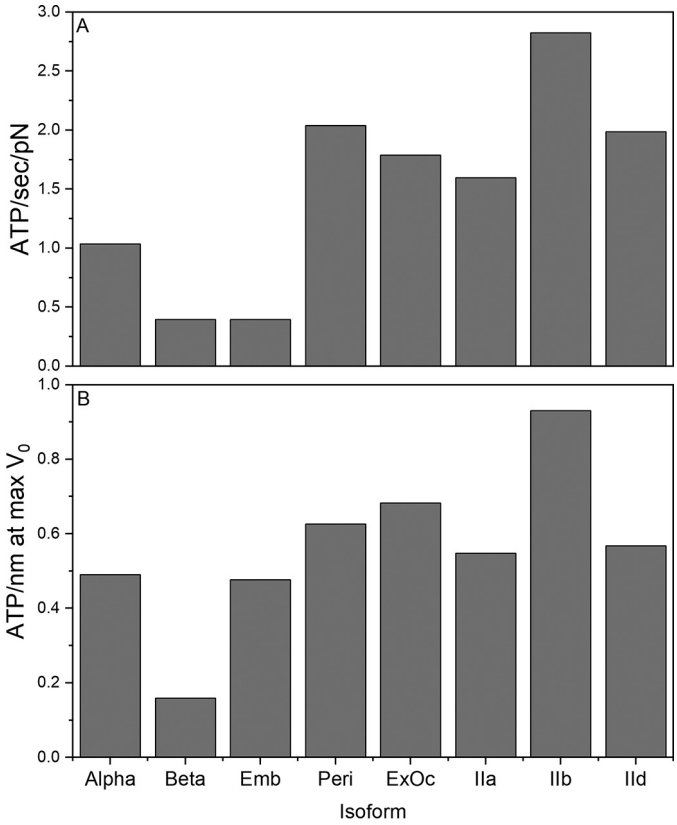

Figure 5. The economy of ATP usage (per myosin head). *A*, when holding a 5-pN load. Economy$_L$ = ATPase (ATP/s)/5 (pN) (where ATPase is estimated at [actin] = 3K_{app}, assuming a similar load dependence for each isoform); *B*, when shortening at V_{max} (V_0) and V_{max} for the ATPase. Economy$_v$ (ATP/nm) = V_{max} (ATP/s)/V_0 (nm/s).

The difference in load sensitivity of the cycle is reflected in the calculation of the economy of the isoforms shown in Fig. 5, which plot ATP used per second when holding a force of 5 pN (Fig. 5*A*) and when shortening at V_{max} and saturating actin (zero load, Fig. 5*B*). At a 5-pN load, both β and Emb myosin have a similar economical usage of ATP (~0.35 ATP/s/pN) and are more economical than α (~3-fold higher ATP usage) or the fast isoforms, which use 1.5–2-fold more ATP than α-myosin for the same load. In contrast, Emb is not as efficient in turning ATPase activity into movement as β-myosin (0.2 ATP/nm of travel) but is similar to α-myosin, which uses just less than 0.5 ATP/nm. Thus, Emb myosin appears to be designed for slow movement but economical force holding. As reported previously, this myosin is also able to continue functioning at much lower ATP concentrations than other myosin isoforms because of tight affinity for ATP (K_T) (8). This property is shared with Peri and, to a lesser extent, with ExOc.

To fully understand the mechanical behavior of a muscle fiber, the force–velocity relationship is required, as this can define the power output (force × velocity) and the velocity at which the power output of the muscle is maximal. This is often

Table 5
Comparison with human muscle fiber data
Values in parenthesis are relative to the type I fiber/β myosin isoform.

Fiber/myosin type	V_0 12 °C[a]	V_0 12 °C[b]	V_0 20 °C[b]	Isometric economy 12 °[b]	Predicted V_0 20 °C	Predicted isometric economy 20 °C
	μm/s/hs	*muscle lengths/s*	*muscle lengths/s*	*μM ATP/s/kN/m²*	*μm/s*	*ATP/nm at max V_0*
I	0.33 ± 0.02 (1.0)	0.37 ± 0.06 (1.0)	1.15 ± 0.36 (1.0)	1	0.2 (1.0)	0.7 (1.0)
IIa	1.40 ± 0.10 (4.2)	0.88 ± 0.12 (2.4)	2.37 ± 0.34 (2.06)	3.5	1.16 (5.8)	1.7 (2.4)
IId	3.02 ± 0.935 (9.15)				1.73 (8.65)	

[a] From Ref. 14.
[b] From Ref. 15.

considered to be the mechanical parameter that defines the optimal operating conditions for a muscle. An equivalent of the force–velocity curve at the single-molecule level has recently been developed, which shows how point mutations and small molecules can alter the relationship (29). Extrapolation between single molecule and whole fiber force–velocity curves is not trivial due to interactions between motors in the ensemble and the elasticity of the sarcomere filament. Thus, our data cannot be used at present to predict the force–velocity relationship. However, the sarcomeric version of the MUSICO program is in principle capable of generating the force–velocity relationship (9). Modeling using this approach is a longer-term project.

Our predictions can be compared, to a limited extent, with the published data on human muscle fibers, where the myosin isoforms present are well-defined. He *et al.* (15) studied the force–velocity and ATPase properties of slow and type IIa human muscle fibers containing only β-myosin and myosin IIa, respectively. Data were collected at 12 and 20 °C, and they calculated the economy of ATPase usage and the optimum velocities for power output. Pellegrino *et al.* (14) additionally reported the velocities of human type I, IIa, and IId/x fibers at 12 °C (and velocities for the same set of fibers from mice, rats, and rabbits). These studies therefore provide detailed muscle fiber data that can be compared with the predictions from our study. That said, there are assumptions built into any extrapolation from solution biochemistry to a muscle fiber that limit direct comparison. These include the number of myosin heads present and fully activated in a muscle fiber, which in turn depends upon the density and packing of filaments in the muscle fiber. The units used to report velocities and ATPases differ due to these corrections. We will therefore limit ourselves to the values of the parameters relative to the values reported for Type 1 fibers containing β-myosin.

Table 5 lists the relative values of V_0, ATPase, and ATP economy under isometric conditions, provided by Pellegrino *et al.* (14) and He *et al.* (15). The relative values of V_0 at 12 °C for Type IIa fibers relative to Type I were 4.2 for Pellegrino *et al.* (14) and 2.4 for He *et al.* (15) He *et al.* (15) had a similar ratio at 20 °C of 2.06. Our data give a ratio nearer to that of Pellegrino of 5.8 for type IIa and 8.65 for type IId, compared with Pellegrino's value of 9.15. Given the degree of error in each of these experimental measurements, the values are of the correct order of magnitude. Similarly, He *et al.* measured the economy of ATP usage by type I fibers to be 3.5-fold better than that of type IIa fibers. In contrast, we calculate a 2.4-fold difference for the two types of myosin.

Overview

Our modeling has revealed distinct characteristics of the ATPase cycle or each of the human isoforms studied. Differences lie in the overall speed of the ATPase cycle (k_{cat}) and the balance of the events in the cycle, which affects how much time the myosin spends at each point of the cycle. There are three significant events in the cycle that define the characteristics of the cycle. 1) the P_i release step (k_{Pi}) controls entry into the strong actin-binding, force-holding states. This event is shown as a single step but probably involves a myosin conformational change before or after the P_i release itself (30, 31). 2) The ADP release step, controlled by the isomerization (k_{D^*}), is followed by rapid ADP release, rapid ATP binding, and then actin dissociation. Thus, the ADP-coupled isomerization is linked to detachment of the cross-bridge. 3) Finally, the ATP hydrolysis step limits how long the cross-bridge remains detached before again being available to bind actin as A-M·D·P_i, which then gives access to the P_i release and force-generating step. All other events are far more rapid, and steps such as nucleotide binding/release and actin binding and release can be treated as rapid equilibration steps. Each of the myosins has a unique relationship between k_{cat} and the three events, which is simply illustrated in Table 4 by showing the value of k_{cat} for each isoform and the value of each of the other rate constants relative to k_{cat}. The values listed give some indication of the contribution of each transition to k_{cat}. In all cases, at least one of the three values is ~2 times k_{cat}, highlighted with a *gray background* in Table 4. This is k_{Pi} in most cases, but for β and Peri, the value of k_H is smaller or comparable with k_{Pi}. A second value for each myosin is ~3–5 times k_{cat} (*yellow background*). This is k_H for all fast isoforms and α, whereas it is k_{D^*} for Emb and k_{Pi} for β and Peri. The third value is ~10 times k_{cat}, and this is k_{D^*} in most cases except Emb. The value for α stands out, as this is ~5 times k_{cat} and similar to the value of k_H. These different relationships between the three constants define the mechanical properties of the isoforms.

The isometric force of muscle fibers is normally found to be relatively invariant within the limits of the precision of the measurement and proportional to the number of strongly attached cross-bridges, although a contribution of weakly attached bridges cannot be ruled out. If this is true, then P_0 will be a function of the number of active bridges and the DR. If all bridges are active (a function of Ca^{2+} activation, force activation, the superrelaxed states, and phosphorylation effects, none of which operates in our pure S1 and actin system), then P_0 is a function of DR. In our hands, the DR is a function of the actin

concentration, and the estimate of P_0 will depend on the effective actin concentration present in the fiber. For a truly isometric fiber, the actin concentration may not be the same for every myosin head due to the mismatch of the actin and myosin filament helices in a muscle. For this reason, we presented our data at different actin concentrations.

Our data show that the DR varies between isoforms: 0.05–0.075 for fast isoforms and 0.1–0.15 for slow/cardiac (even higher for Emb). Thus, the expected P_0 values per myosin head will be proportional to these DR values. Of course, in the fiber, the myosins act as an ensemble, and the mechanical coupling between myosin may alter these numbers. In addition, whereas the density of thick filaments in a muscle fiber may be similar for all fast muscles, variations in packing are expected in slow and developing muscle, where cell contents are not so exclusively packed with myofilaments.

The predicted V_0 values vary in a way roughly compatible with expectation; the velocities are expected to be independent of actin concentration and so should be independent of the packing of filaments in the fiber. However, a question remains of whether unloaded shortening truly exists in the muscle fiber, where some internal load may always be present, and therefore measured values will underestimate the true V_0. Comparison of V_0 muscle fiber values with motility velocities rarely shows exact correspondence for reasons not yet fully explained, although myosin orientation on the surface and the exact make up of actin filaments are thought to play a part in such discrepancies (32).

A limitation of our analysis is the limited data available on the load dependence of myosin isoforms. In the absence of experimental data, we have made the simplifying assumption that the load dependence is the same in each case. Although this assumption may not be true, our modeling does illustrate how differences in the cycle alone can generate different load sensitivities for the isoforms. Force–velocity curves for muscle fibers in principle contain the information on load dependence but are not available for many fibers containing a single myosin isoforms.

The solution data do not currently allow us to generate a force–velocity curve, which would be required to define the optimal velocity for power output for each myosin type. This is believed to be the condition where the muscle is designed to operate. V_0 and P_0 will provide the end points for the force–velocity curve, but the shape of the relationship is distinct for different fibers and may depend on internal muscle elastic elements in addition to the ATPase cycle of different myosin motor domains. Single molecule methods or loaded motility assays could be used to measure the load dependence of individual myosin isoforms. This will reveal whether the myosin motor domain itself defines the shape of the force–velocity curve.

In common with most studies of myosin in solution our data are collected at 20 °C and 25 mM KCl as the reference conditions. These are some way from the physiological conditions of 0.15–0.17 M ionic strength and 37 °C. The conditions stated above are needed to allow accurate measurement of the ATPase and motility data and to allow comparison with muscle fiber mechanics. Extrapolation to physiological conditions is possible for the well-defined β-cardiac myosin and adult fast-muscle myosin, where there are extensive data on the temperature and salt dependence of many of the parameters. For all other isoforms, no such data currently exist.

Our analysis of the differences in the cross-bridge cycle for each myosin isoform raises the issue of the sequence changes that bring about the adaptations to function. Earlier studies have examined groups of isoforms to identify key sequence changes (18, 33-35). These have often emphasized the variable surface loops in which isoform-specific sequence changes occur. However, the source of the sequence changes required to bring about the changes in the overall balance of the cross-bridge cycle is likely to be more widespread. We show a sequence alignment of the eight human isoforms in Fig. S5 and outline the major areas where changes occur in the legend to the figure. These span several regions: (i) residues 302–339, an area that corresponds to one of the alternate spliced regions in the Drosophila muscle myosins; (ii) actin-binding loop 3 (residues 561–579) and loop 4 (residues near 370); and (iii) helix O (residues 425–451) in the upper 50-kDa domain. These areas are of interest because the same areas were highlighted in a study of the sequence variation of the β-cardiac myosin motor domain associated with changes in velocity between mammals (36). Future analyses will include a combination of bioinformatics, modeling, and experimental investigation to define the sequences that generate the different properties of sarcomeric myosins and are responsible for their functional diversity.

Materials and methods

Protein expression and purification

Human muscle MyHC-sS1 for the β-isoform and MyHC-S1 for the α-isoform were expressed and purified as described previously (6). The motor domain of the β heavy chain was co-expressed with the N-terminal His_6-tagged, human essential light chain MYL3. The motor domain of the Emb myosin isoform was expressed with a His_6 tag on the C terminus (8). The fast-muscle isoforms (IIb, IId, and IIa), Peri, and ExOc isoforms were expressed with a C-terminally fused enhanced GFP and His_6 tag. All proteins carrying a C-terminal His_6 tag when purified carried the endogenous mouse light chains present in the C2C12 cells (see Table 1) (21). Briefly, replication-incompetent recombinant adenoviruses were produced using the pAdEasy system containing expression cassettes encoding S1 of the human myosins under the transcriptional control of a cytomegalovirus promoter. The adenoviral particles were amplified using HEK293 cells; the viruses were purified using CsCl gradients, and the concentrated virus was stored in a glycerol buffer at −20 °C. These adenoviruses were used to infect C_2C_{12} myotubes in culture, and cells were collected and frozen into cell pellets. Pellets were then homogenized in a low-salt buffer and centrifuged, and the supernatants were purified by affinity chromatography using a HisTrap HP 1-ml column. The proteins were then dialyzed into the low-salt experimental buffer (25 mM KCl, 20 mM MOPS, 5 mM $MgCl_2$, 1 mM DTT, pH 7.0).

Actin was prepared from rabbit muscle as described previously (37). The actin was labeled with pyrene at Cys-374 as described previously (38). When used at submicromolar con-

centrations, the actin was stabilized by incubation in a 1:1 mixture with phalloidin.

Kinetic measurements

Fast kinetic data for every isoform except for the Peri isoform have been published previously (6–8). All kinetic measurements for the Peri isoform were performed as described previously (6–8). Solutions were buffered with 20 mM MOPS, 5 mM $MgCl_2$, 25 mM KCl, 1 mM DTT at pH 7.0, and measurements were conducted at 20 °C on a High-Tech Scientific SF-61 DX2 stopped-flow system. Traces were analyzed in Kinetic Studio (TgK Scientific) and Origin (OriginLab). The experimental data for all isoforms are summarized in Table S1. ATPase data for Peri, ExOc, IIa, IIb, and IId isoforms were performed at 37 °C (21). To calculate the expected k_{cat} values at 20 °C, a Q_{10} value of 1.5 was used (27).

Modeling

The published set of rate and equilibrium constants is summarized in Table S1, together with the k_{cat} and K_{app} values from steady-state actin-activated ATPase assays. With these data, the eight-state actin·myosin ATPase cycle was modeled using the MUSICO software as described (9, 10). The eight-step scheme of Fig. 1 has a total of 24 rate and equilibrium constants, but not all are independent. For each step, i, $K_i = k_i/k_{-i}$, and thus only two of the constants need to be defined experimentally for a complete description of the cycle. The free energy of ATP hydrolysis further constrains the overall balance of the cycle. Experiments have defined forward rate constants k_{D^*}, k_{T^*}, and k_H and the equilibrium constants K_T and either K_D or $K_D K_{D^*}$, in most cases to a precision of at least 20% (see Table S1). The rate constants k_{-T^*} and k_D are defined as diffusion-limited. The events $k_{T^{**}}$ and k_{-A} are considered too fast to measure and thus have little effect on the modeling. Fitting the model to the actin-dependent steady-state ATPase data can give estimates for the equilibrium constants for actin binding (K_A), ATP hydrolysis (K_H), and on-actin hydrolysis step (K_{AH}) and the rate constants for phosphate release and ATP dissociation (k_{Pi} and k_T, respectively). The $K_i = k_i/k_{-i}$ detailed balance equation can be used to define K_{T^*}, k_A, k_{-Pi}, k_{-D^*}, k_{-D}, k_{-T}, k_{-H}, and k_{-AH}. The initial concentration of ATP was set at 5 mM, and those of ADP and P_i were set at 0 mM; under steady-state conditions, these are assumed to be zero.

The fraction of myosin in the strongly attached states AMD, AM-D, AM, and AMT in the steady state is defined as the DR. From the DR, an estimate of the maximal velocity, V_0, can be calculated from Equation 1, where d is the distance over which myosin can produce force, and τ is the lifetime of the strongly attached state. The lifetime of the attached state is equal to DR/ATPase rate; hence, $V_0 = d$·ATPase/DR. The economy, or the amount of ATP used per myosin per nm of travel when the ATPase and the velocity are maximal, can be derived from Economy_V (ATP/nm) = V_{max} (ATP/s)/V_0 (nm/s).

In our previous modeling, we used the data from two laboratories that used single-molecule laser trap methods to define the effect of load on the ADP release step of the cycle (k_{D^*}) (12, 13). These indicated that for β-cardiac, a 5-pN load on actin·myosin slowed the ADP release by ~3-fold. A similar effect on the power stroke (coupled to P_i release in our eight-state model) is also required to slow the ATPase cycling by ~3-fold, as reported for muscle fibers under isometric conditions (15). Here, in the absence of any direct measurements on any other isoform, we make the assumption that all isoforms have a similar load dependence. Whereas this is an oversimplification, it does allows us to illustrate how load affects each isoform differently due to the changed balance of events in the cycle. To estimate the economy of ATP usage per pN of force generated at any actin concentration, the ATPase rate was divided by the load, here 5 pN.

Error analysis

The sensitivity matrices shown in Table S3 demonstrate that with the exception of k_{-T}, the fitted parameters are all well-defined in the modeling program; values in the diagonal of >0.8 indicate well-resolved parameters with little codependence. As reported previously (9), varying one of the fitted parameters (k_H, k_{-D}, $K_D{}^*$, k_{-D^*}, k_{-T^*}, or K_{T^*}) by ±20% has minimal effect on the best-fit values for the remaining parameters. This observation remained true for the data presented in this study (see Table S4 for analysis of the Emb data), with the remaining parameters varying by much less than 20%, with a few exceptions.

In our previous paper on DCM mutations in β-cardiac myosin, we also explored the effect of a 20% error in the value of V_{max} (k_{cat}) or K_{app} used in the fitting. These again showed that the data are reasonably robust. K_{app} is primarily defined by the value of K_A, and a 20% change in K_{app} has little effect on the cycle apart from a change in K_A. This is also because we model the data at different actin concentration related to K_A. Changes in V_{max} will change the flux round the cycle. V_{max} is largely controlled by a combination of k_{Pi} and k_H, depending upon the isoform, and these will adjust as the k_H changes by 20%. If k_{AMD} does not change and we use our measured value, then the occupancy of AMD must change to increase or decrease the flux through this state to match the altered V_{max}. Thus, AMD will change by some fraction of 20% but no more than this. A 20% change is within the tolerance we claim for the overall precision of the cycle and will not alter substantially the pattern seen for each isoform.

Author contributions—C. A. J., M. A. G., and L. A. L. conceived the study. C. A. J., with M. S. and S. M. M., completed the kinetic modeling. J. W. designed, performed, and analyzed the stopped-flow experiments on the perinatal protein provided by C. D. V. and A. K. All authors contributed to the final version of the manuscript.

References

1. Acakpo-Satchivi, L. J. R., Edelmann, W., Sartorius, C., Lu, B. D., Wahr, P. A., Watkins, S. C., Metzger, J. M., Leinwand, L., and Kucherlapati, R. (1997) Growth and muscle defects in mice lacking adult myosin heavy chain genes. *J. Cell Biol.* **139,** 1219–1229 CrossRef Medline
2. Oldfors, A. (2007) Hereditary myosin myopathies. *Neuromuscul. Disord.* **17,** 355–367 CrossRef Medline
3. Haraksingh, R. R., Jahanbani, F., Rodriguez-Paris, J., Gelernter, J., Nadeau, K. C., Oghalai, J. S., Schrijver, I., and Snyder, M. P. (2014) Exome sequencing and genome-wide copy number variant mapping reveal novel associ-

ations with sensorineural hereditary hearing loss. *BMC Genomics* **15,** 1155 CrossRef Medline
4. Schiaffino, S., and Reggiani, C. (2011) Fiber types in mammalian skeletal muscles. *Physiol. Rev.* **91,** 1447–1531 CrossRef Medline
5. Bottinelli, R., and Reggiani, C. (2000) Human skeletal muscle fibres: molecular and functional diversity. *Prog. Biophys. Mol. Biol.* **73,** 195–262 CrossRef Medline
6. Deacon, J. C., Bloemink, M. J., Rezavandi, H., Geeves, M. A., and Leinwand, L. A. (2012) Erratum to: Identification of functional differences between recombinant human α and β cardiac myosin motors. *Cell Mol. Life Sci.* **69,** 4239–4255 CrossRef Medline
7. Bloemink, M. J., Deacon, J. C., Resnicow, D. I., Leinwand, L. A., and Geeves, M. A. (2013) The superfast human extraocular myosin is kinetically distinct from the fast skeletal IIa, IIb, and IId isoforms. *J. Biol. Chem.* **288,** 27469–27479 CrossRef Medline
8. Walklate, J., Vera, C., Bloemink, M. J., Geeves, M. A., and Leinwand, L. (2016) The most prevalent freeman-sheldon syndrome mutations in the embryonic myosin motor share functional defects. *J. Biol. Chem.* **291,** 10318–10331 CrossRef Medline
9. Mijailovich, S. M., Nedic, D., Svicevic, M., Stojanovic, B., Walklate, J., Ujfalusi, Z., and Geeves, M. A. (2017) Modeling the actin.myosin ATPase cross-bridge cycle for skeletal and cardiac muscle myosin isoforms. *Biophys. J.* **112,** 984–996 CrossRef Medline
10. Ujfalusi, Z., Vera, C. D., Mijailovich, S. M., Svicevic, M., Yu, E. C., Kawana, M., Ruppel, K. M., Spudich, J. A., Geeves, M. A., and Leinwand, L. A. (2018) Dilated cardiomyopathy myosin mutants have reduced force-generating capacity. *J. Biol. Chem.* **293,** 9017–9029 CrossRef Medline
11. VanBuren, P., Harris, D. E., Alpert, N. R., and Warshaw, D. M. (1995) Cardiac V1 and V3 myosins differ in their hydrolytic and mechanical activities *in vitro*. *Circ. Res.* **77,** 439–444 CrossRef Medline
12. Greenberg, M. J., Shuman, H., and Ostap, E. M. (2014) Inherent force-dependent properties of β-cardiac myosin contribute to the force-Velocity relationship of cardiac muscle. *Biophys. J.* **107,** L41–L44 CrossRef Medline
13. Sung, J., Nag, S., Mortensen, K. I., Vestergaard, C. L., Sutton, S., Ruppel, K., Flyvbjerg, H., and Spudich, J. A. (2015) Harmonic force spectroscopy measures load-dependent kinetics of individual human β-cardiac myosin molecules. *Nat. Commun.* **6,** 7931 CrossRef Medline
14. Pellegrino, M. A., Canepari, M., Rossi, R., D'Antona, G., Reggiani, C., and Bottinelli, R. (2003) Orthologous myosin isoforms and scaling of shortening velocity with body size in mouse, rat, rabbit and human muscles. *J. Physiol.* **546,** 677–689 CrossRef Medline
15. He, Z. H., Bottinelli, R., Pellegrino, M. A., Ferenczi, M. A., and Reggiani, C. (2000) ATP consumption and efficiency of human single muscle fibers with different myosin isoform composition. *Biophys. J.* **79,** 945–961 CrossRef Medline
16. Schiaffino, S., Rossi, A. C., Smerdu, V., Leinwand, L. A., and Reggiani, C. (2015) Developmental myosins: Expression patterns and functional significance. *Skelet. Muscle* **5,** 22 CrossRef Medline
17. Bloemink, M. J., and Geeves, M. A. (2011) Shaking the myosin family tree: biochemical kinetics defines four types of myosin motor. *Semin. Cell Dev. Biol.* **22,** 961–967 CrossRef Medline
18. Weiss, A., Schiaffino, S., and Leinwand, L. A. (1999) Comparative sequence analysis of the complete human sarcomeric myosin heavy chain family: implications for functional diversity. *J. Mol. Biol.* **290,** 61–75 CrossRef Medline
19. Brueckner, J. K., Itkis, O., and Porter, J. D. (1996) Spatial and temporal patterns of myosin heavy chain expression in developing rat extraocular muscle. *J. Muscle Res. Cell Motil.* **17,** 297–312 Medline
20. Sartore, S., Mascarello, F., Rowlerson, A., Gorza, L., Ausoni, S., Vianello, M., and Schiaffino, S. (1987) Fibre types in extraocular muscles: a new myosin isoform in the fast fibres. *J. Muscle Res. Cell Motil.* **8,** 161–172 CrossRef Medline
21. Resnicow, D. I., Deacon, J. C., Warrick, H. M., Spudich, J. A., and Leinwand, L. A. (2010) Functional diversity among a family of human skeletal muscle myosin motors. *Proc. Natl. Acad. Sci. U.S.A.* **107,** 1053–1058 CrossRef Medline
22. Nag, S., Sommese, R. F., Ujfalusi, Z., Combs, A., Langer, S., Sutton, S., Leinwand, L. A., Geeves, M. A., Ruppel, K. M., and Spudich, J. A. (2015) Contractility parameters of human β-cardiac myosin with the hypertrophic cardiomyopathy mutation R403Q show loss of motor function. *Sci. Adv.* **1,** e1500511 CrossRef Medline
23. Walklate, J., and Geeves, M. (2015) Temperature manifold for a stopped-flow machine to allow measurements from −10 to +40 °C. *Anal. Biochem.* **476,** 11–16 CrossRef Medline
24. Bloemink, M. J., Adamek, N., Reggiani, C., and Geeves, M. A. (2007) Kinetic analysis of the slow skeletal myosin MHC-1 isoform from bovine masseter muscle. *J. Mol. Biol.* **373,** 1184–1197 CrossRef Medline
25. Iorga, B., Adamek, N., and Geeves, M. (2007) The slow skeletal muscle isoform of myosin shows kinetic features common to smooth and non-muscle myosins. *J. Biol. Chem.* **282,** 3559–3570 CrossRef Medline
26. White, H. D., and Taylor, E. W. (1976) Energetics and mechanism of actomyosin adenosine triphosphatase. *Biochemistry* **15,** 5818–5826 CrossRef Medline
27. Siemankowski, R. F., Wiseman, M. O., and White, H. (1985) ADP dissociation from actomyosin subfragment 1 is sufficiently slow to limit the unloaded shortening velocity in vertebrate muscle. *Proc. Natl. Acad. Sci. U.S.A.* **82,** 658–662 CrossRef Medline
28. Sleep, J. A., and Hutton, R. L. (1980) Exchange between inorganic phosphate and adenosine 5′-triphosphate in the medium by actomyosin subfragment 1. *Biochemistry* **19,** 1276–1283 CrossRef Medline
29. Liu, C., Kawana, M., Song, D., Ruppel, K. M., and Spudich, J. A. (2018) Controlling load-dependent kinetics of β-cardiac myosin at the single-molecule level. *Nat. Struct. Mol. Biol.* **25,** 505–514 CrossRef Medline
30. Houdusse, A., and Sweeney, H. L. (2016) How myosin generates force on actin filaments. *Trends Biochem. Sci.* **41,** 989–997 CrossRef Medline
31. Muretta, J. M., Rohde, J. A., Johnsrud, D. O., Cornea, S., and Thomas, D. D. (2015) Direct real-time detection of the structural and biochemical events in the myosin power stroke. *Proc. Natl. Acad. Sci. U.S.A.* **112,** 14272–14277 CrossRef Medline
32. Homsher, E., Wang, F., and Sellers, J. R. (1992) Factors affecting movement of F-actin filaments propelled by skeletal muscle heavy meromyosin. *Am. J. Physiol.* **262,** C714–C723 CrossRef Medline
33. Alpert, N. R., Brosseau, C., Federico, A., Krenz, M., Robbins, J., and Warshaw, D. M. (2002) Molecular mechanics of mouse cardiac myosin isoforms. *Am. J. Physiol. Heart Circ. Physiol.* **283,** H1446–H1454 CrossRef Medline
34. Chikuni, K., Muroya, S., Tanabe, R., and Nakajima, I. (2003) Comparative sequence analysis of four myosin heavy chain isoforms expressed in porcine skeletal muscles: sequencing and characterization of the porcine myosin heavy chain slow isoform. *Anim. Sci. J.* **73,** 257–262 CrossRef
35. Toniolo, L., Patruno, M., Maccatrozzo, L., Pellegrino, M. A., Canepari, M., Rossi, R., D'Antona, G., Bottinelli, R., Reggiani, C., and Mascarello, F. (2004) Fast fibres in a large animal: fibre types, contractile properties and myosin expression in pig skeletal muscles. *J. Exp. Biol.* **207,** 1875–1886 CrossRef Medline
36. Johnson, C. A., Mcgreig, J. E., Vera, C. D., Mulvihill, D. P., Ridout, M., Leinwand, L. A., Wass, M. N., and Geeves, M. A. (2019) Cardiac contraction velocity has evolved to match heart rate with body size through variation in β-cardiac myosin sequence. *bioRxiv* CrossRef
37. Spudich, J. A., and Watt, S. (1971) The regulation of rabbit skeletal muscle contraction. I. Biochemical studies of the interaction of the tropomyosin-troponin complex with actin and the proteolytic fragments of myosin. *J. Biol. Chem.* **246,** 4866–4871 Medline
38. Criddle, A. H., Geeves, M. A., and Jeffries, T. (1985) The use of actin labelled with *N*-(1-pyrenyl)iodoacetamide to study the interaction of actin with myosin subfragments and troponin/tropomyosin. *Biochem. J.* **232,** 343–349 CrossRef Medline